



# Design and analysis of an underwater inductive coupling power transfer system for autonomous underwater vehicle docking applications<sup>\*</sup>

Jian-guang SHI, De-jun LI<sup>‡</sup>, Can-jun YANG

(State Key Laboratory of Fluid Power Transmission and Control, Hangzhou 310027, China)

E-mail: swortex@gmail.com; li\_dejun@zju.edu.cn; ycj@zju.edu.cn

Received June 24, 2013; Revision accepted Oct. 12, 2013; Crosschecked Dec. 19, 2013

**Abstract:** We develop a new kind of underwater inductive coupling power transfer (ICPT) system to evaluate wireless power transfer in autonomous underwater vehicle (AUV) docking applications. Parameters that determine the performance of the system are systematically analyzed through mathematical methods. A circuit simulation model and a finite element analysis (FEA) simulation model are developed to study the power losses of the system, including copper loss in coils, semiconductor loss in circuits, and eddy current loss in transmission media. The characteristics of the power losses can provide guidelines to improve the efficiency of ICPT systems. Calculation results and simulation results are validated by relevant experiments of the prototype system. The output power of the prototype system is up to 45 W and the efficiency is up to 0.84. The preliminary results indicate that the efficiency will increase as the transmission power is raised by increasing the input voltage. When the output power reaches 500 W, the efficiency is expected to exceed 0.94. The efficiency can be further improved by choosing proper semiconductors and coils. The analysis methods prove effective in predicting the performance of similar ICPT systems and should be useful in designing new systems.

**Key words:** Inductive coupling power transfer (ICPT), Autonomous underwater vehicle (AUV) docking, Coupling coefficient, Resonant capacitance, Power transfer efficiency, Power loss, Eddy current

doi:10.1631/jzus.C1300171

Document code: A

CLC number: TM131.4<sup>†</sup>1

## 1 Introduction

Autonomous underwater vehicle (AUV) docking technology is a quickly developing field. The goal is to recharge AUVs from submerged docks in deep sea environments, thus prolonging an AUV's endurance time. Connector design for underwater power delivery is a major challenge in AUV docking technology. The position of the docked AUV is difficult to maintain, and the docking station is submerged in sea

water for a long period of time, making the use of plugged connectors impractical. A wireless connector has been proven to be a better choice because it does not need to be plugged in and has no pins exposed to seawater, and thus has a high tolerance to fouling and corrosion (Podder *et al.*, 2004; McEwen *et al.*, 2008; Pyle *et al.*, 2012).

A leading candidate to achieve wireless power transfer is inductive coupling, a method applied to many types of terrestrial devices, such as vehicle charge (Villa *et al.*, 2012), radar power supply (Papastergiou and Macpherson, 2007a), and portable electronic devices charge (Ota *et al.*, 2011). Inductive coupling power transfer (ICPT) devices have also been applied to underwater environments to charge AUVs (Kojiya *et al.*, 2004; Han *et al.*, 2007) and

<sup>‡</sup> Corresponding author

<sup>\*</sup> Project supported by the National High-Tech R&D Program of China (No. 2013AA09A414), the National Natural Science Foundation of China (No. 51221004), and the Interdisciplinary Research Foundation of Zhejiang University (No. 2012HY003A)

© Zhejiang University and Springer-Verlag Berlin Heidelberg 2014

profilers (Howe *et al.*, 2006). Unlike common transformers, ICPT devices are loosely coupled, leading to leakage inductance and increased power loss. Thus, assessing the overall efficiency of ICPT devices is very important. In the literature, efficiency is primarily evaluated by experimental measurements (Kojiya *et al.*, 2004; Han *et al.*, 2007; Papastergiou and Macpherson, 2007a; Li *et al.*, 2010). A few studies (Taheri *et al.*, 2011; Zargham and Gulak, 2012; Sibue *et al.*, 2013) addressed the efficiency issue from a loss perspective to define efficiency-related factors, in order to predict the efficiency of a certain type of ICPT system. In a typical underwater inductive coupling power transfer (UICPT) system, there are three types of power loss, namely copper loss in coils, semiconductor loss in circuits, and eddy current loss in transmission media. It is important to define their contributions to system efficiency calculations. Zargham and Gulak (2012) assessed the power loss of a near-field coupled system through biological media with simulation methods. Sibue *et al.* (2013) proposed a 3D finite element method to introduce the computation of losses in conductors and magnetic cores of a 1.6 kW–100 kHz ICPT system. Taheri *et al.* (2011) studied the core loss and copper loss of a transformer through a 3D finite element method. The simulation methods in the literature have not integrated the circuits in a finite element analysis (FEA) model, making them differ from the practical system, and semiconductor loss and eddy current loss in sea water have not been mentioned. In this paper, we evaluate the characteristics of all the three types of loss, and introduce the detailed mathematical model, circuit analysis model, and circuit-integrated FEA model for loss evaluation.

Another important issue of the ICPT system is power transfer ability, a characteristic closely related to the system's resonant state and usually measured by output power (Kojiya *et al.*, 2004; Low *et al.*, 2009). The factors that affect the output power of an ICPT system are studied through a mathematical model and techniques to enhance power transfer ability are suggested in this paper.

The design goal of our UICPT system is to deliver over 500 W power between two coils that are installed in a docking system submerged in a 1000-m-deep sea environment with the highest efficiency possible. The UICPT system consists of a transmit-

ting circuit, a receiving circuit, and an electromagnetic (EM) coupler, which are designed specifically for AUV docking applications.

To evaluate the requirement, a prototype UICPT system enabling 50 W power transfer under water has been built. Due to the diversity of ICPT systems, it is impossible to achieve a result that can be applied to all types of ICPT systems. All the studies in this paper are based on the specific prototype system and extended to predict the performance of relevant UICPT systems and determine techniques for further improvement. Hopefully, the analytical approaches applied and the results achieved will assist in designing other ICPT systems and underwater devices.

The objectives of this study are to (1) design an inductive power transfer system specifically for AUV docking applications, (2) evaluate the performance of the system through theoretical analysis, (3) determine the effect of all the parameters on the performance of the system for further improvement, and (4) verify the viability of the system and the accuracy of analysis results through experiments.

## 2 System design

To optimize the structure of the docking system, the EM coupler is designed to be composed of two coaxial coils with large diameters, one installed on the external aluminum shell of an AUV and the other inside a docking cone. Fig. 1 shows the installation of the coils in an AUV docking system. The docking system functions as follows: the AUV locates the position of the docking station and enters the docking station through the cone, then the AUV is locked in position, and electric power is transferred from the docking station to the AUV through the UICPT to charge the AUV's batteries.

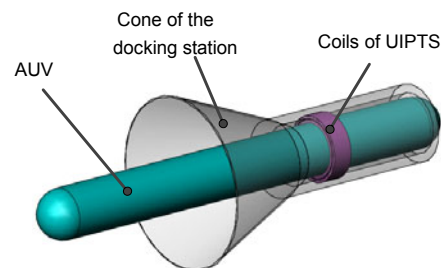
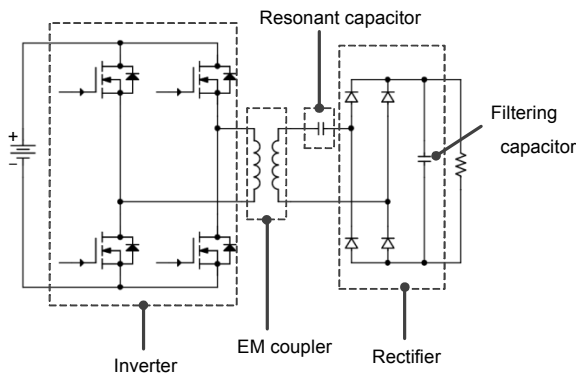


Fig. 1 Installation of the coils

The circuit layout of the UICPT system is shown in Fig. 2. It is composed of four primary components: inverter, EM coupler, resonant capacitor, and rectifier. The inverter consisting of four pulse-width modulation (PWM) controlled MOSFETs combines the parasitic capacitances of the MOSFETs and the parasitic inductance of the EM coupler to achieve zero voltage switching (ZVS) using a phase shift full bridge (PSFB) topology (Papastergiou and Macpherson, 2007b). Resonant capacitance is necessary to reduce the phase shift between load voltage and load current to maximize the effective power transferred by a UICPT system. Several types of compensation methods have been previously investigated, suggesting different characteristics for various applications (Wang *et al.*, 2004; Kim and Jin, 2012; Villa *et al.*, 2012). In this study, to ensure the reliability of the system, compensation with a series capacitor in the secondary side is selected (the resonant capacitor in Fig. 2).



**Fig. 2** Circuit layout of the underwater inductive coupling power transfer (UICPT) system

The components of the prototype circuit are selected according to the design requirements. The PWM control signal is generated by a PWM generating chip (UCC3895, Unitrode, USA), whose frequency can be adjusted by a variable resistor connected to it. IRFP260N MOSFETs (IR, USA) are selected to build the inverter. The parasitic capacitances in these MOSFETs help to achieve ZVS. In the rectifier circuit, MUR1620CT (SHANGHAI LUN-SURE, China) diodes are used.

The coils are wound with Litz wires to reduce their AC resistances. The diameters of the coils are determined by the structure of the docking system, and are 282 mm and 300 mm in this example. The diameter of the transmitting coil is larger to allow the

AUV wearing the receiving coil to enter the dock opening in the docking station. The turn numbers of the primary coils and the secondary coils are 10 and 20, respectively. Self-inductances and AC resistances of the coils are primary concerns in determining these parameters. First, we determine the secondary inductance to be around 200  $\mu\text{H}$  and frequency to be around 150 kHz according to our previous work (Li *et al.*, 2010). Then the turn number is estimated using the formula given by Howe *et al.* (2006). Considering the poor coupling condition, the turn ratio of 1:2 is chosen to maintain the output voltage. The parameters of the coils are further verified by calculating the AC resistances using the formula proposed by Hurley *et al.* (2000). The results turn out to be acceptable. The resonant capacitance is chosen according to the desired inductances and the frequency to achieve the resonant state, using the formula introduced by Ghahary and Cho (1992). As the capacitance needs to be standard, the value of 10 nF is chosen and the resonant state is established by adjusting the frequency to 167 kHz.

After the prototype coils are fabricated, the parameters are measured with an LCR meter. The AC resistances of the primary coil and the secondary coil are 0.3  $\Omega$  and 0.7  $\Omega$ , respectively, at the frequency of 167 kHz. The measured inductances of the primary coil and the secondary coil are 70  $\mu\text{H}$  and 210  $\mu\text{H}$ , respectively, and the mutual inductance  $M$  between them is 90  $\mu\text{H}$ . Consequently, the coupling coefficient can be calculated using  $k = M / \sqrt{L_1 L_2}$ , which comes to 0.74. The parameters of the prototype system are summarized in Table 1, which will be further referred to in the following analysis.

**Table 1** Parameters of the prototype system

Parameter	Value
Frequency, $f$	167 kHz
Input voltage, $V_1$	45 V
Coupling coefficient, $k$	0.74
Resonant capacitance, $C$	10 nF
Primary AC resistance, $R_1$	0.3 $\Omega$
Secondary AC resistance, $R_2$	0.7 $\Omega$
Primary inductance, $L_1$	70 $\mu\text{H}$
Secondary inductance, $L_2$	210 $\mu\text{H}$
Load resistance, $R_0$	50 $\Omega$

### 3 Theoretical analysis

When considering the performance of a UICPT system, the primary performance measures are power delivery ability and overall efficiency. In this case, power delivery ability is determined by the output power when a constant voltage source is applied. Overall efficiency relates to power losses in all the components and transmission media, including copper loss in the coils, semiconductor loss in the circuits, and eddy current loss in sea water and the AUV shell. A theoretical evaluation of these components and their losses is presented in this section.

#### 3.1 Evaluation of the EM coupler

The EM coupler plays a key role in determining the performance of a UICPT system. In this case, as compensation with a series capacitor in the secondary side is adopted, the EM coupler shows some special characteristics, which will be analyzed in detail in this subsection.

Hysteresis loss normally present in common EM couplers is avoided in this design by use of the coreless coils. Eddy current loss is determined by the electromagnetic field of the EM coupler and the conductivity of the transmission media, and both can be separated from the EM coupler's major characteristics. Thus, to evaluate the performance of the EM coupler, only copper loss and the power factor are considered. Fig. 3 illustrates a simplified circuit of the UICPT system. The power source is simplified by a sinusoidal voltage source, the load is simplified by a resistance, and the EM coupler is modeled by two resistances and a mutual inductor.

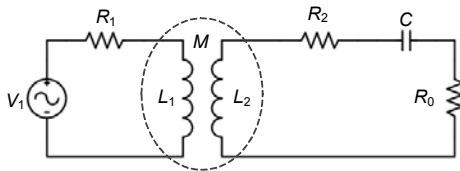


**Fig. 3** Simplified circuit of the underwater inductive coupling power transfer (UICPT) system

The symbols in Fig. 3 are consistent with those listed in Table 1.  $M$  is the mutual inductance between the two coils,  $M = k\sqrt{L_1 L_2}$ . The input power can be calculated using

$$P_1 = V_1 I_1 \cos \phi, \quad (1)$$

where  $I_1$  is the current through the primary circuit, and  $\phi$  is the phase difference between  $V_1$  and  $I_1$ . According to Ohm's law, the current through the primary circuit is given by

$$I_1 = V_1 / Z_{11}, \quad (2)$$

where  $Z_{11}$  is the equivalent impedance in the primary circuit. It comprises the resistance  $R_1$ , the inductive reactance  $j\omega L_1$  ( $\omega$  is the angular frequency of the sinusoidal voltage source), and the reflected impedance of the secondary circuit  $Z_i$ .

$$Z_{11} = R_1 + j\omega L_1 + Z_i. \quad (3)$$

The reflected impedance of the secondary circuit is related to the total impedance of the secondary circuit  $Z_{22}$ , the mutual inductance  $M$ , and the angular frequency  $\omega$ :

$$Z_i = (\omega M)^2 / Z_{22}. \quad (4)$$

The impedance of the secondary circuit comprises load resistance  $R_0$ , secondary AC resistant  $R_2$ , inductive reactance  $j\omega L_2$ , and capacitive reactance  $-1/(j\omega C)$ .

$$Z_{22} = R_0 + R_2 + j\omega L_2 - 1/(j\omega C). \quad (5)$$

The output power  $P_2$  on the load can be calculated by

$$P_2 = I_2^2 R_0, \quad (6)$$

where  $I_2$  is the current through the load resistance, calculated from

$$I_2 = j\omega M / Z_{22} \cdot I_1. \quad (7)$$

Now that once the input power and output power are obtained, the efficiency of the EM coupler,  $\eta$ , can be calculated by  $\eta = P_2 / P_1$ .

We have tried to solve the above equations and express  $P_1$  and  $P_2$  with the known parameters. However, the result is rather complicated and shows few clues. Thus, software package MATLAB was used to perform numerical calculations of the equation set.

Eqs. (1)–(7) are written into a MATLAB program to study the influence of the parameters on the performance of the EM coupler. The method first assigns an initial value to each parameter and then sets the parameters inspected as variables to study their relationship with efficiency or output power. The initial values of the parameters are exactly the same as those of the prototype UICPT system, as listed in Table 1.

The circuit of a UICPT system is supposed to work under a nearly resonant state to achieve the maximum power output. Circuit frequency, resonant capacitance, and the coupling coefficient are the primary factors that affect the power factor. Since the coupling coefficient is an independent value that relates only to the property of an EM coupler, the other two factors are initially set as variables and their effects are assessed. Their effect on the output power is illustrated in Fig. 4. It can be seen that if either value of the parameters is frozen, there is a corresponding specific value of the other parameter necessary to achieve the maximum output power. For example, when the capacitance is frozen at 17 nF, the necessary frequency value is 125 kHz. In addition, the maximum output power changes little when frequency drops, which indicates that the system can work properly in the inspected range. Based on this result, the resonant capacitance and frequency we have chosen for our prototype UICPT system may not be an optimal choice. Larger capacitance and lower frequency can still maintain the magnitude of the output power, while losses may be reduced by decreasing the frequency to a value lower than 167 kHz.

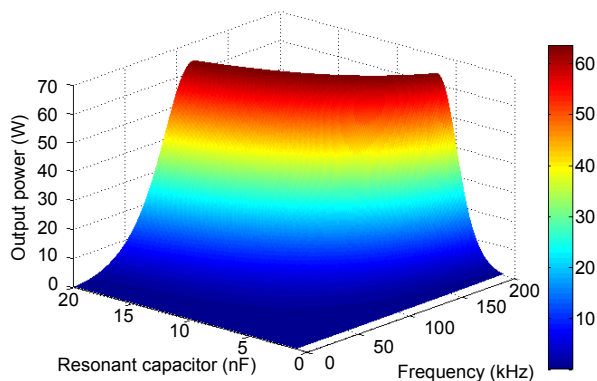


**Fig. 4** Output power as a function of resonant capacitance and frequency

The coupling coefficient is an important EM coupler parameter. In this case, the coefficient should be relatively low due to the coreless design and the gap between the two coils. Thus, it is important to determine which role the coupling coefficient plays in power delivery.

Because the coupling coefficient affects the power factor of a UICPT system, the capacitance is adjusted during the analysis to maintain the system in a nearly resonant state. The system frequency is fixed at 167 kHz during the analysis.

According to the calculation results, the coupling coefficient has little impact on efficiency, but it does contribute to the output characteristics of the EM coupler (Fig. 5). A larger coupling coefficient promises better power transfer ability but not manifestly higher efficiency, particularly when the coefficient exceeds 0.5.

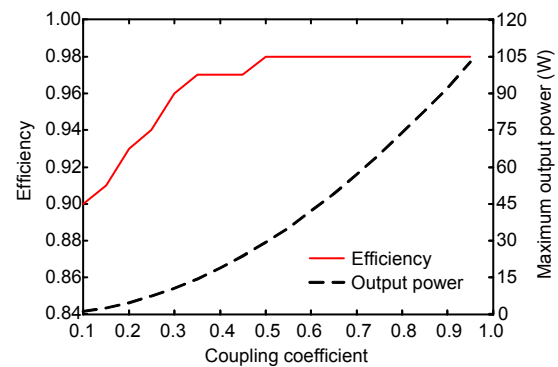
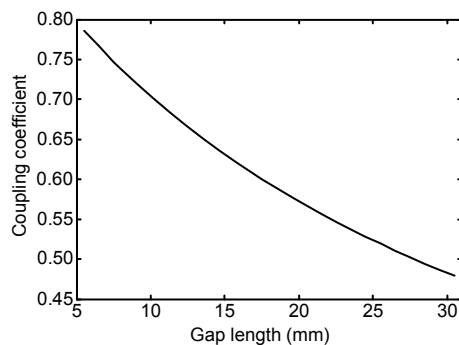


**Fig. 5** Maximum power output and corresponding efficiency with respect to the coupling coefficient

The left vertical axis of the plot represents the system efficiency when the maximum output power is achieved. The maximum power output is obtained by adjusting the resonant capacitor to reach a resonant state for a specific coupling coefficient

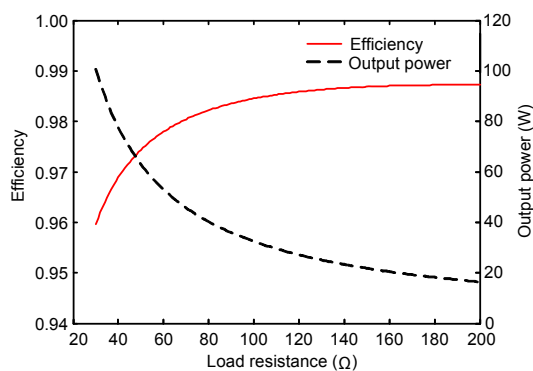
The coupling coefficient is significantly affected by the relative position of the coils. In this design, the coils are coaxially placed, so the significant variable is the gap length between the coils. Computation methods (Babic and Akyel, 2000) have been developed to calculate the coupling coefficient between two coaxial coils, whereas the process is a bit complicated. Here we recommend the FEA method, which proves simple and accurate. To study the change in the coupling coefficient under different gap lengths, a 2D simulation model is built using the FEA software package ANSOFT MAXWELL and a

magnetostatic analysis is performed. The simulation results illustrated in Fig. 6 can be combined with Fig. 5 to assess the performance of an EM coupler. The coupling coefficient drops moderately as the gap length increases, resulting in a decline of power transfer ability, and efficiency is less affected during the process. For example, when the gap increases to 30 mm, the coupling coefficient reduces to 0.5. In the meantime, the efficiency stays at 0.98 and the maximum output power drops to 29 W.



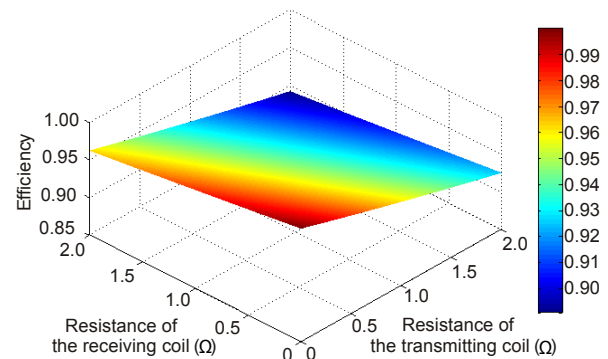
**Fig. 6** Coupling coefficient with respect to gap length between coils

Fig. 7 illustrates the efficiency and the output power of the EM coupler under different load conditions. As expected, an increase in load resistance results in a decrease in output power and an increase in efficiency. Note that although the increasing trend of the efficiency is clear, the overall change in efficiency is less than 0.03, indicating that the load resistance has a minor effect on efficiency. Although the maximum output power values are observed for load resistance values lower than 25  $\Omega$ , these are not displayed in the plot.



**Fig. 7** Efficiency and output power of the EM coupler versus load resistance

The efficiency of the EM coupler is also affected by the parameters of the coils, that is, AC resistance and self-inductance. The AC resistances of the transmitting coil and receiving coil both show a nearly linear relationship with coupler efficiency (Fig. 8). In comparison, the self-inductances of the coils have little effect on coupler efficiency as long as their values are not too low (Fig. 9). On the other hand, self-inductances are closely related to output power (Fig. 10). The output power shows nearly linear



**Fig. 8** Influence of the AC resistances of coils on efficiency

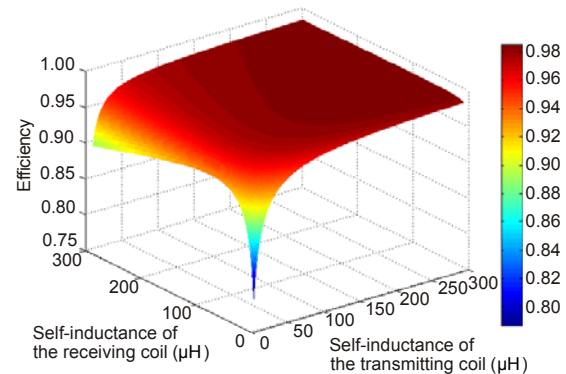


**Fig. 9** Influence of the self-inductances of coils on efficiency

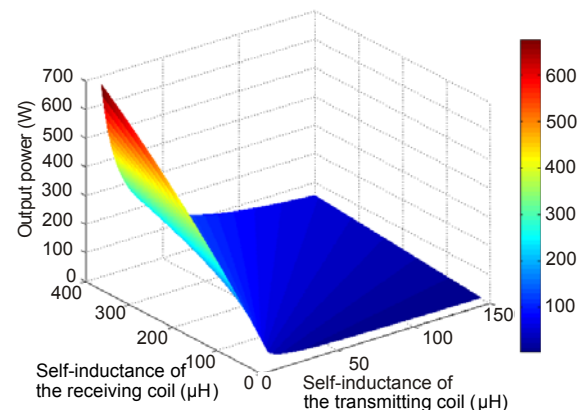


**Fig. 10** Influence of the self-inductances of coils on output power



relationship with the ratio of  $L_2$  to  $L_1$ . As a result, reducing  $L_1$  or increasing  $L_2$  is a measure to improve power transfer ability. Note that Figs. 9 and 10 are derived when resonant state is maintained by adjusting the resonant capacitance.

### 3.2 Eddy current loss

Considering the application environment of the proposed UICPT system, eddy current loss, caused by the fast changing magnetic field of the EM coupler, occurs in the shell of the AUV and the sea water between the coils. Both the primary and secondary coils can incur eddy current, making the problem complicated and difficult to solve using traditional calculation methods. Thus, to evaluate the influence of eddy current on system performance, a simulation model is built using the FEA software package ANSYS. As the coils of the UICPT system are axially symmetric, a 2D model is effective for this analysis. Fig. 11 shows the layout of the model in the FEA domain.

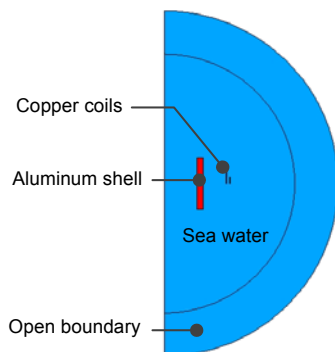


**Fig. 11** Layout of the finite element analysis (FEA) domain of the simulation model

The left rectangle represents the aluminum autonomous underwater vehicle (AUV) shell. The copper coils are placed outside the AUV shell. There is a gap between the inner coil and the AUV shell for installation of the former (in practical use, this gap is filled with ABS material). The gap between the two coils is 9 mm. Sea water fills the remaining space of the model.

A circuit model is attached to the FEA domain to provide excitation. A pulse voltage of 45 V and a frequency of 167 kHz are assigned to the outer coil (the transmitting coil). A load of 50  $\Omega$  is specified and a series capacitor of 10 nF is attached to model the receiving coil.

The simulation results of eddy current loss in the

aluminum shell and in sea water (Fig. 12) reveal the fluctuation of eddy current loss from 18  $\mu$ s to 36  $\mu$ s during the simulation, when the UICPT system operates at a stable state. Eddy current loss is relatively small compared to the output power. Despite the high conductivity of the aluminum shell, the eddy current loss in the shell is much smaller than that in sea water. An explanation of this phenomenon is that a relatively large gap exists between the shell and the inner coil, thus reducing the magnetic field intensity throughout the shell. In addition, although these two curves have the same cycle period, they fluctuate in different ways. This may be caused by the different positions of the two media. The shell is affected more intensely by the secondary coil than by the primary coil, because it is more close to the former. In contrast, sea water sees no difference between the coils.

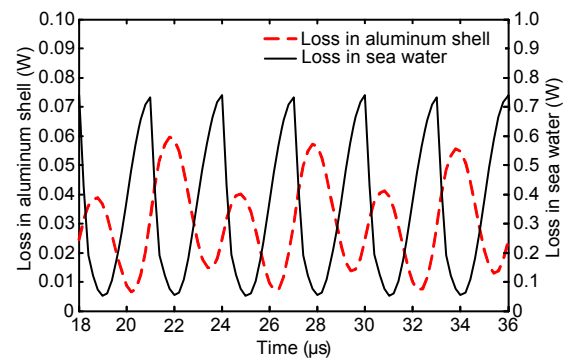


**Fig. 12** Eddy current loss fluctuation during steady state power transfer

Mean losses based on three cycles have been calculated from the simulation results, totaling 0.03 W in the aluminum shell and 0.34 W in sea water. Note that the corresponding mean output power is 43.49 W.

To further study the characteristics of eddy current loss, its distribution over the cross sections of sea water and the aluminum shell is plotted in Figs. 13 and 14, respectively. Each plot is derived when eddy current loss reaches its maximum value in a cycle. These two plots indicate that eddy current loss exists mainly in the area that surrounds the coils for sea water, and in the outer layer for the aluminum shell (on the right side in Fig. 13), in agreement with skin effect theory.

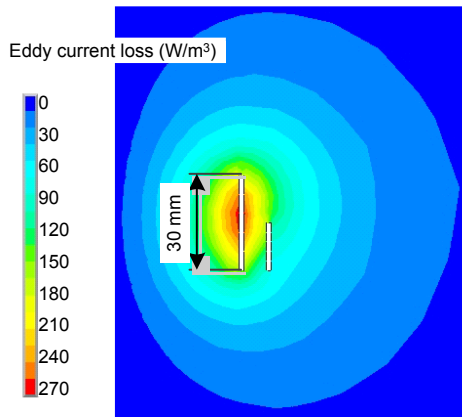


**Fig. 13** Eddy current loss distribution in a cross section of sea water

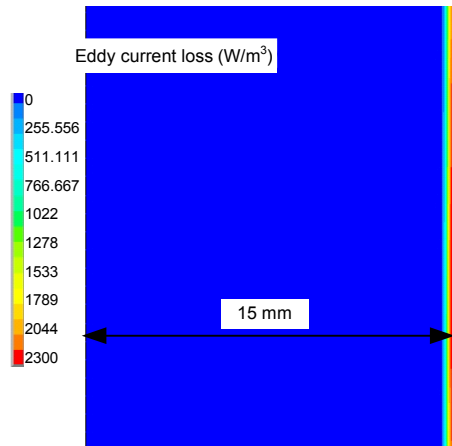


**Fig. 14** Eddy current loss distribution in a cross section of the aluminum shell

### 3.3 Loss in circuits

In general, to deliver DC power through two coupling coils, an inverter and a rectifier are required to change DC current into AC current and to change AC current back into DC current. Power loss occurs in the semiconductors of these circuits, namely MOSFETs and diodes. Calculating semiconductor losses is complicated and the calculation results are inaccurate, due to the characteristics of semiconductors and the complexity of the circuits. Hence, PSPICE, the widely used circuit analysis tool, is selected to study the semiconductor losses in the circuits. Initially, the components are modeled in the software according to the data provided by the manufacturers. Then the circuits are constructed in the exact configuration as the prototype UICPT system (Fig. 2), except that the filtering capacitor is omitted. This

simplification is based on two reasons. First, much longer simulation time will be required if the filtering capacitor is present, because the capacitor needs to be fully charged before the system reaches a stable state. Second, as there is no power loss in the capacitor, the simplification does not influence the efficiency analysis.

The EM coupler is simulated by a transformer. The static drain-to-source on-resistance of the selected MOSFET type is  $0.04 \Omega$  and the maximum forward voltage drop of the selected diode type is  $0.975 \text{ V}$ . All other parameters are set to be exactly the same as those of the prototype system, as listed in Table 1.

The simulation results of the input power, output power, and copper loss in the coils are first compared with the calculation results to verify that they are mutually confirmed. Then the simulation results of the semiconductor losses in the MOSFETs and diodes (Figs. 15 and 16) indicate the fluctuation of power loss in one of the MOSFETs and one of the diodes, respectively. The peaks in Fig. 15 represent the turn-off loss of the MOSFET. The negative values are

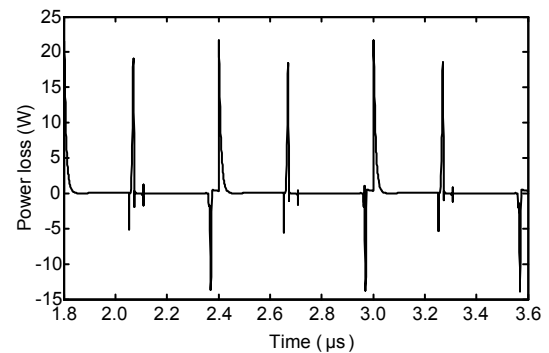


**Fig. 15** Power loss fluctuation in one of the MOSFETs during steady state power transfer

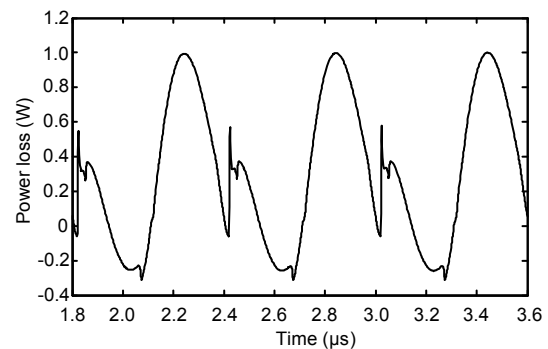


**Fig. 16** Power loss fluctuation in one of the diodes during steady state power transfer



supposed to be caused by the parasitic capacitance of the component. The total average power loss is 1.6 W for the combined four MOSFETs and 1.2 W for the four diodes. Considering the average output power of 43.5 W, the total loss of 2.8 W is acceptable. Nevertheless, by applying alternate semiconductors or improving circuit layout, it is possible to further reduce the semiconductor circuit loss if necessary.

### 3.4 High power UICPT system

The above analysis is based on a fixed input voltage and with limited maximum output power. To fulfill the objective of designing a high power UICPT system, enhancement of the input voltage is necessary. In this analysis, the load resistance is fixed at 50  $\Omega$  and various input voltages are assigned to study the efficiency of the UICPT system in high output power conditions. As input voltage has nothing to do with the power factor, a nearly resonant state of the system is maintained during the process. Fig. 17 illustrates the changes in the three types of losses (copper loss, semiconductor loss, and eddy current loss) with respect to the output power.

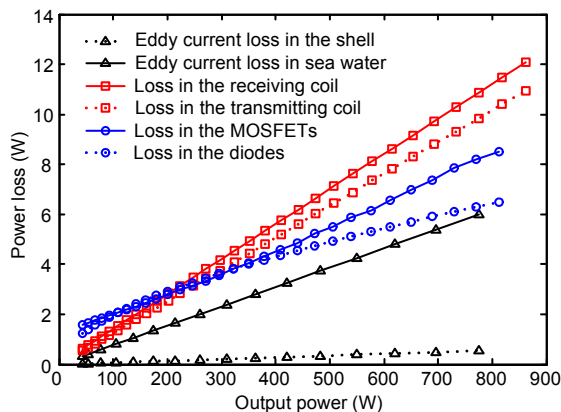


Fig. 17 Losses under different output power conditions at various input voltages

The curves of the losses in the coils and semiconductors are obtained by circuit simulation, where eddy current loss is not taken into account. The curves of eddy current losses are obtained through transient electromagnetic field FEA simulation, where semiconductor loss is not taken into account. Although these constraints may reduce the accuracy of the analysis results, the implied losses represent a small portion of the total consumed power, so the results are

still useful in assessing the efficiency of a high power UICPT system.

Except the loss in the diodes whose growth rate slows as output power increases, the other types of losses all increase nearly linearly with output power. Eddy current loss is relatively small compared to the other losses. Semiconductor loss represents the major loss when the output power is low. As the output power increases, the copper loss grows and exceeds the semiconductor loss. Because none of the lines has a slope greater than 1, the efficiency of the system is assumed to increase as output power increases. When the output power is 500 W, the efficiency is expected to exceed 0.94.

## 4 Experimental validation

Calculation and FEA methods are very effective in system design due to their ability to give relatively accurate prediction of the characteristics of UICPT systems by allowing examination of various parameters. However, to verify the accuracy of a mathematic model or FEA model, relevant experiments are necessary. Thus, several experiments were carried out using the prototype UICPT system. Fig. 18 shows the coils immersed in simulated sea water.

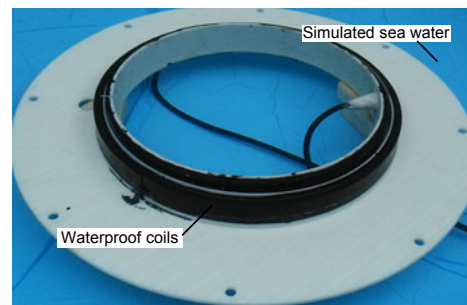
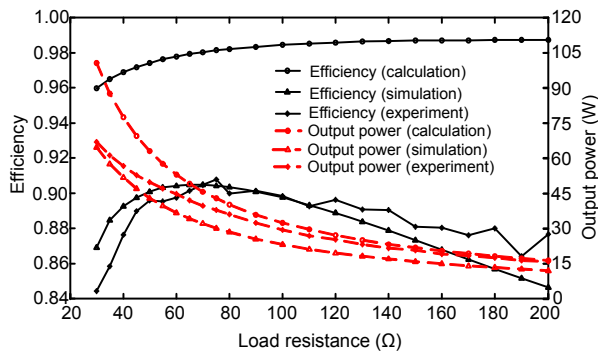


Fig. 18 Photograph of the test coils

The EM coupler was first placed in air to assess the efficiency of the circuits and the coils. All the parameters of the components were calibrated to ensure consistency between the analysis models and the prototype. The only variable is thus the load resistance.

The input power and output power under different load conditions were recorded, and the overall efficiency of the system was obtained. Fig. 19 shows

a comparison among calculation results, circuit simulation results, and experiment results. The output power curves show similar declining trends as load resistance increases; meanwhile, the gaps between them remain in a reasonable range. In reality, the components in a practical UICPT system are not ideal, and a small change in capacitance or system frequency can impact the resonant state, resulting in fluctuations in the output power. In addition, semiconductor loss is not taken into account in the calculation analysis. These may explain the discrepancies among the power curves.



**Fig. 19** Comparison of efficiency and output power in calculation, circuit simulation, and experiment results

The layout of the circuit simulation model and that of the prototype are roughly the same. Both contain two types of loss, semiconductor loss and copper loss; thus, they produce similar results regarding efficiency and output power. On the other hand, the absence of semiconductor loss in the calculation analysis produces a high efficiency curve. This phenomenon reveals the important role that semiconductor loss plays in determining the overall efficiency of the UICPT system when the input voltage is low, consistent with the results shown in Fig. 16. Indeed, the effect of semiconductor loss will decrease as input voltage increases.

The effectiveness of the calculation analysis and circuit simulation analysis was verified by the above experiment. Then, the experiment was repeated with the EM coupler placed outside an aluminum shell in simulated sea water (with conductivity of 4.3 s/m) to imitate the actual application environment of the UICPT system, where eddy current loss exists. The experiment results for efficiency and output power were compared with the FEA results (Fig. 20). The

results of the first experiment, in which eddy currents did not exist, were also added to the plots to compare the performance of the prototype system when it was placed in different applications. In general, FEA results regarding output power agreed well with the experiment results. Similar to the calculation results, the FEA efficiency results were a little higher than the experiment results due to the absence of semiconductor loss in FEA simulations. Regarding efficiency curve trends, these match well as load resistance increases.

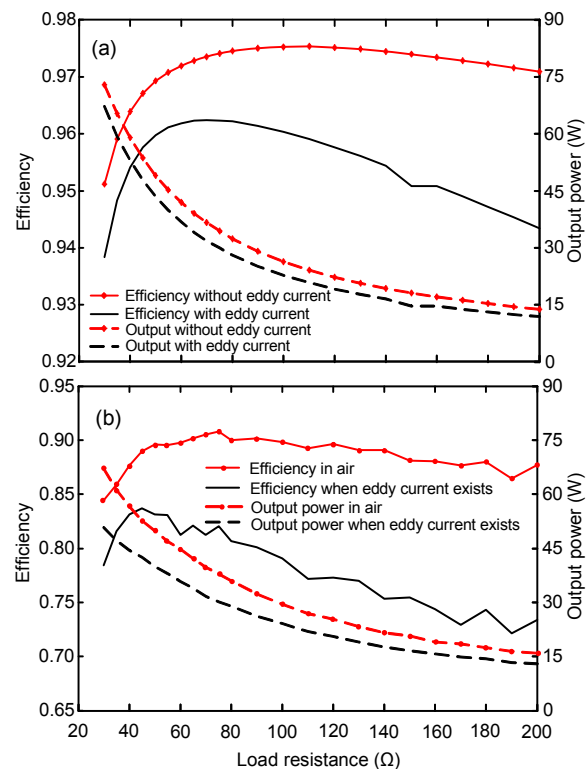


**Fig. 20** Comparison of FEA (a) and experiment (b) results

An interesting phenomenon emerging from the plots is that both FEA results and experiment results indicate a discrepancy much larger than the value of eddy current loss between the output power curves. To explain this phenomenon, several measurements were made. It was found that the self-inductances of the two coils dropped from 70  $\mu\text{H}$  and 210  $\mu\text{H}$  to 61  $\mu\text{H}$  and 177  $\mu\text{H}$ , respectively after the shell was placed in the center of the coils. The output power dropped consequently, according to Fig. 10. The drop of self-inductances is supposed to be caused by the eddy current in the shell (Scott, 1930; Dodd and

Deeds, 1968; Moulder *et al.*, 1998; Dukju and Songcheol, 2013). Yet, there is no systematic theory to predict the inductance of a coil with a core consisting of low-permeability conductors. Further exploration of relevant theories is anticipated in this field.

In both of the above experiments, the relative position of the coils was changed several times in the radial direction. During the process, the input and output power remained constant. These results demonstrate that the radial movement of the AUV (which is only axially fixed) during the power transfer process will not interfere with the operation of the UICPT system. In other words, the relative radial position of the coils has no effect on the coupling coefficient, thus confirming the reliability of the EM coupler shown in Fig. 1.

## 5 Conclusions

UICPT represents a promising system for transfer of power between a docking station and a docked AUV. A prototype UICPT system is proposed and its properties are studied. The following conclusions are drawn:

1. In the circuit topology applied in this design, there is a resonant capacitance corresponding to a certain frequency that produces the maximum power output.
2. The coupling coefficient between the coils is found to affect the maximum output power, but has little effect on the efficiency.
3. Copper loss is affected by the AC resistances of the coils and the load resistance. Thus, to reduce copper loss, feasible solutions are to reduce AC resistances by applying proper wires with low AC resistance or by reducing the system's resonant frequency.
4. Semiconductor loss is determined by the properties of the applied MOSFETs and diodes and can be reduced by selecting suitable components.
5. Eddy current losses generated in sea water and in the aluminum shell are relatively small compared with the other two losses, as long as the gap between the shell and the inner coil is wide enough. However, the effect of the conductive shell on the self-inductances of the coils is an important issue that

should be considered in UICPT design.

6. There are two effective ways to enhance output power: one is to raise input voltage, and the other is to select proper inductances of the coils according to Fig. 10.

The analysis methods are verified by comparing the calculation results and simulation results of efficiency and output power with experiment results using a prototype UICPT system. Further improvement of the prototype UICPT system will be performed based on the analysis results.

## References

- Babic, S., Akyel, C., 2000. Improvement in calculation of the self- and mutual inductance of thin-wall solenoids and disk coils. *IEEE Trans. Magn.*, **36**(4):1970-1975. [doi:10.1109/TMAG.2000.875240]
- Dodd, C.V., Deeds, W.E., 1968. Analytical solutions to eddy current probe coil problems. *J. Appl. Phys.*, **39**(6):2829-2838. [doi:10.1063/1.1656680]
- Dukju, A., Songcheol, H., 2013. A study on magnetic field repeater in wireless power transfer. *IEEE Trans. Ind. Electron.*, **60**(1):360-371. [doi:10.1109/TIE.2012.2188254]
- Ghahary, A., Cho, B.H., 1992. Design of transcutaneous energy transmission system using a series resonant converter. *IEEE Trans. Ind. Electron.*, **7**(2):261-269. [doi:10.1109/63.136242]
- Han, J., Asada, A., Ura, T., *et al.*, 2007. Noncontact power supply for seafloor geodetic observing robot system. *J. Mar. Sci. Tech.*, **12**(3):183-189. [doi:10.1007/s00773-006-0235-4]
- Howe, B.M., McGinnis, T., Gobat, J., 2006. Moorings for ocean observatories: continuous and adaptive sampling. *Scientific Submarine Cable Conf.*, p.172-181.
- Hurley, W.G., Gath, E., Breslin, J.G., 2000. Optimizing the AC resistance of multilayer transformer windings with arbitrary current waveforms. *IEEE Trans. Power Electron.*, **15**(2):369-376. [doi:10.1109/63.838110]
- Kim, Y.H., Jin, K.H., 2012. A contactless power transfer system using a series-series-parallel resonant converter. *Int. J. Electron.*, **99**(7):885-897. [doi:10.1080/00207217.2011.653947]
- Kojiya, T., Sato, F., Matsuki, H., *et al.*, 2004. Automatic power supply system to underwater vehicles utilizing non-contacting technology. *Oceans*, p.2341-2345. [doi:10.1109/OCEANS.2004.1406521]
- Li, Z., Li, D., Lin, L., *et al.*, 2010. Design considerations for electromagnetic couplers in contactless power transmission systems for deep-sea applications. *J. Zhejiang Univ-Sci. C (Comput. & Electron.)*, **11**(10):824-834. [doi:10.1631/jzus.C0910711]
- Low, Z.N., Chinga, R.A., Tseng, R., *et al.*, 2009. Design and test of a high-power high-efficiency loosely coupled

- planar wireless power transfer system. *IEEE Trans. Ind. Electron.*, **56**(5):1801-1812. [doi:10.1109/TIE.2008.2010110]
- McEwen, R.S., Hobson, B.W., McBride, L., et al., 2008. Docking control system for a 54-cm-diameter (21-in) AUV. *IEEE J. Ocean. Eng.*, **33**(4):550-562. [doi:10.1109/JOE.2008.2005348]
- Moulder, J.C., Tai, C.C., Larson, B.F., et al., 1998. Inductance of a coil on a thick ferromagnetic metal plate. *IEEE Trans. Magn.*, **34**(2):505-514. [doi:10.1109/20.661482]
- Ota, Y., Takura, T., Sato, F., et al., 2011. Impedance matching method about multiple contactless power feeding system for portable electronic devices. *IEEE Trans. Magn.*, **47**(10):4235-4237. [doi:10.1109/TMAG.2011.2156399]
- Papastergiou, K.D., Macpherson, D.E., 2007a. An airborne radar power supply with contactless transfer of energy. Part I: rotating transformer. *IEEE Trans. Ind. Electron.*, **54**(5):2874-2884. [doi:10.1109/TIE.2007.902044]
- Papastergiou, K.D., Macpherson, D.E., 2007b. An airborne radar power supply with contactless transfer of energy. Part II: converter design. *IEEE Trans. Ind. Electron.*, **54**(5):2885-2893. [doi:10.1109/TIE.2007.901370]
- Podder, T., Sibenac, M., Bellingham, J., 2004. AUV docking system for sustainable science missions. *IEEE Int. Conf. on Robotics & Automation*, p.4478-4484. [doi:10.1109/ROBOT.2004.1302423]
- Pyle, D., Granger, R., Geoghegan, B., et al., 2012. Leveraging a large UUV platform with a docking station to enable forward basing and persistence for light weight AUVs. *Oceans*, p.1-8. [doi:10.1109/OCEANS.2012.6404932]
- Scott, K.L., 1930. Variation of the inductance of coils due to the magnetic shielding effect of eddy currents in the cores. *Proc. IRE*, **18**(10):1750-1764. [doi:10.1109/JRPROC.1930.221920]
- Sibue, J.R., Meunier, G., Ferrieux, J.P., et al., 2013. Modeling and computation of losses in conductors and magnetic cores of a large air gap transformer dedicated to contactless energy transfer. *IEEE Trans. Magn.*, **49**(1):586-590. [doi:10.1109/TMAG.2012.2211031]
- Taheri, S., Gholami, A., Fofana, I., et al., 2011. Modeling and simulation of transformer loading capability and hot spot temperature under harmonic conditions. *Electr. Power Syst. Res.*, **86**:68-75. [doi:10.1016/j.epsr.2011.12.005]
- Villa, J.L., Sallan, J., Sanz Osorio, J.F., et al., 2012. High-misalignment tolerant compensation topology for ICPT systems. *IEEE Trans. Ind. Electron.*, **59**(2):945-951. [doi:10.1109/TIE.2011.2161055]
- Wang, C.S., Covic, G.A., Stielau, O.H., 2004. Power transfer capability and bifurcation phenomena of loosely coupled inductive power transfer systems. *IEEE Trans. Ind. Electron.*, **51**(1):148-157. [doi:10.1109/TIE.2003.822038]
- Zargham, M., Gulak, P.G., 2012. Maximum achievable efficiency in near-field coupled power-transfer systems. *IEEE Trans. Biomed. Circ. Syst.*, **6**(3):228-245. [doi:10.1109/TBCAS.2011.2174794]

### Recommended paper related to this topic

#### **Design considerations for electromagnetic couplers in contactless power transmission systems for deep-sea applications**

Authors: Ze-song Li, De-jun Li, Lin Lin, Ying Chen

doi:10.1631/jzus.C0910711

*Journal of Zhejiang University-SCIENCE C (Computers & Electronics)*, 2010 Vol.11 No.10 P.824-834

**Abstract:** In underwater applications of contactless power transmission (CLPT) systems, high pressure and noncoaxial operations will change the parameters of electromagnetic (EM) couplers. As a result, the system will divert from its optimum performance. Using a reluctance modeling method, we investigated the gap effects on the EM coupler in deep-sea environment. Calculations and measurements were performed to analyze the influence of high pressure and noncoaxial alignments on the coupler. It was shown that it is useful to set a relatively large gap between cores to reduce the influence of pressure. Experiments were carried out to verify the transferring capacity of the designed coupler and system for a fixed frequency. The results showed that an EM coupler with a large gap can serve a stable and efficient power transmission for the CLPT system. The designed system can transfer more than 400 W electrical power with a 2-mm gap in the EM coupler, and the efficiency was up to 90% coaxially and 87% non-coaxially in 40 MPa salt water. Finally, a mechanical layout of a 400 W EM coupler for the underwater application in 4000-m deep sea was proposed.